ULUSLARARASI 3B YAZICI TEKNOLOJİLERİ
VE DİJİTAL ENDÜSTRİ DERGİSİ

INTERNATIONAL JOURNAL OF 3D PRINTING TECHNOLOGIES AND DIGITAL INDUSTRY

ISSN:2602-3350 (Online)

URL: https://dergipark.org.tr/ij3dptdi

POROSITY-DEPENDENT METALLIZATION AND SUBSEQUENT STRENGTHENING OF ADDITIVELY MANUFACTURED POROUS POLYMER LATTICES

Yazarlar (Authors): Nihan Sengokmen-Ozsoz*

Bu makaleye şu şekilde atıfta bulunabilirsiniz (To cite to this article): *Sengokmen Ozsoz N., "Porosity-Dependent Metallization and Subsequent Strengthening of Additively Manufactured Porous Polymer Lattices" Int. J. of 3D Printing Tech. Dig. Ind., 10(1): 135-143, (2026).*

DOI: 10.46519/ij3dptdi.1813114

Araştırma Makale/ Research Article

Erişim Linki: (To link to this article): https://dergipark.org.tr/en/pub/ij3dptdi/archive

POROSITY-DEPENDENT METALLIZATION AND SUBSEQUENT STRENGTHENING OF ADDITIVELY MANUFACTURED POROUS POLYMER LATTICES

Nihan Sengokmen-Ozsoz[a]*

[a]Gebze Technical University, Faculty of Engineering, Department of Materials Science and Engineering, TURKEY

* *Corresponding Author:* nihans.ozsoz@gtu.edu.tr

(**Received:** 29.10.25; **Revised:** 28.03.26; **Accepted:** 15.04.26)

ABSTRACT

The use of polymerized high internal phase emulsions (polyHIPEs) combined with electroless nickel plating provides an effective route to fabricate architected porous polymers with enhanced structural performance. The resulting metallized lattices exhibit low density, high stiffness, and improved interfacial integrity, making them suitable for lightweight structural, catalytic, and energy-related applications. This study investigates the influence of porosity on metallization and mechanical reinforcement in 3D-printed polyHIPE lattices. A water-in-oil HIPE was used as a vat-photopolymerizable resin and printed via digital light processing (DLP) into lattice structures with target porosities of 80% and 87.5%, followed by electroless nickel coating. SEM revealed open-cell, interconnected morphologies with average pore sizes of 35.15 ± 17.47 µm (P80) and 41.55 ± 14.20 µm (P87.5). Surface and cross-sectional SEM/EDS confirmed uniform nickel deposition with penetration depths of 83 ± 21 µm (P80Ni) and 199 ± 86 µm (P87.5Ni), indicating more effective coating at higher porosity. Compression testing showed a compressive modulus increase from 0.27 ± 0.06 kPa for the polymer lattices to 159.70 ± 29.26 kPa and an ~85-fold increase in compressive strength after metallization. These results reveal a clear structure–property relationship between porosity, coating depth, and mechanical performance, demonstrating that electroless nickel plating effectively transforms lightweight polyHIPE lattices into robust, multifunctional architected materials.

Keywords: PolyHIPE, Electroless Metallization, Vat Photopolymerization, Porous Lattices

1. INTRODUCTION

Porous polymeric structures have attracted increasing attention due to their unique properties, including low density, high surface area, and tunable pore architectures. These materials have been investigated for applications in thermal insulation, energy storage, catalysis, adsorption, and biomedical scaffolds [1-3]. Within this class, polymerized high internal phase emulsions (polyHIPEs) represent a versatile family of emulsion-templated porous polymers characterized by interconnected, open-cell morphologies and high porosities exceeding 74% [4-6].

Conventional manufacturing methods, such as casting or foaming, are restricted to simple geometries and often lack control over hierarchical pore structures [7-8]. In contrast, additive manufacturing (AM) offers unprecedented freedom in designing and fabricating complex porous networks, enabling precise control over pore size, distribution, and architecture [9-10]. Vat photopolymerization (VPP) and material extrusion (MEX) techniques have been successfully combined with HIPE resins to fabricate inherently porous, multiscale structures with enhanced fidelity and functional performance [11-17]. Despite challenges associated with the inherent light-scattering behavior of HIPEs and their rheological complexity, recent advances have enabled the production of intricate polyHIPE scaffolds, lattices, and even trabecular bone replicas [15,17-18].

Beyond their direct use as lightweight porous polymers, polyHIPEs can also serve as

templates for advanced inorganic structures. Additively manufactured polyHIPE lattices have been demonstrated as sacrificial scaffolds for producing metallic or carbon frameworks [15, 17]. In particular, electroless nickel plating has emerged as a cost-effective technique to deposit uniform metallic coatings onto complex polymeric substrates without requiring external electrical power [19-20]. Nickel-coated polyHIPEs exhibit advantageous combinations of low density, high specific strength, resilience, and functional surface properties, making them attractive for applications in battery electrodes, catalytic supports, and acoustic or vibration damping [21-27]. However, while polyHIPE lattices provide an inherently porous template, their mechanical fragility remains a challenge for structural applications, necessitating reinforcement strategies such as metallization.

To date, systematic investigations into the combined effects of porous structure and metallization on the performance of polyHIPE lattices remain limited. In our previous study, the electroless nickel plating of 3D-printed polyHIPEs was optimized and the feasibility of fabricating ultra-porous nickel lattices with retained structural fidelity after template removal was demonstrated [15]. Building on these foundations, subsequent studies have highlighted the importance of understanding the interplay between polyHIPE morphology, coating penetration, and the resulting functional properties [17,18].

In this work, the knowledge gap was addressed by fabricating polyHIPE lattices with controlled porosities (80% and 87.5%) using vat photopolymerization, followed by electroless nickel plating. The morphological, compositional, and mechanical characteristics of the resulting structures were systematically evaluated through scanning electron microscopy (SEM), energy-dispersive spectroscopy (EDS), and uniaxial compression testing. Unlike previous approaches that utilize polyHIPEs primarily as sacrificial templates for purely metallic or metallic/carbon foams, this study focuses on the direct mechanical reinforcement of the intact composite lattice. Furthermore, while existing literature on metallized polyHIPEs has largely relied on simple cylindrical geometries for mechanical testing, our work investigates complex 3D-printed architected lattices, offering a comprehensive evaluation of their porosity-dependent coating penetration and a quantitative assessment of the significant mechanical strengthening effect achieved through metallization. This study provides new insights into the structure–property relationships of metallized polyHIPE lattices, advancing their potential use in lightweight structural and multifunctional applications.

2. MATERIALS AND METHODS

2-ethylhexyl acrylate (EHA), isobornyl acrylate (IBOA), trimethylolpropane triacrylate (TMPTA), a photoinitiator; diphenyl (2,4,6-trimethyl benzoyl)-phosphine oxide/2-hydroxy-2-methyl propiophenone (blend), beta carotene (synthetic, ≥93% (UV), powder), and tartrazine (dye content ≥85%), 3-(trimethoxysilyl)propyl methacrylate, tin (II) chloride ($SnCl_2$), palladium (II) chloride ($PdCl_2$), boric acid (H_3BO_3), and ~37% hydrochloric acid (HCl) were all purchased from Sigma Aldrich. The surfactant Hypermer B246-SO-M was donated by Croda. Electroless nickel plating solutions (Part A and Part B) were purchased from Caswell.

2.1. Emulsion Preparation

A continuous organic phase was prepared by mixing 39.70 wt% 2-ethylhexyl acrylate (EHA), 39.70 wt% isobornyl acrylate (IBOA), 15.90 wt% trimethylolpropane triacrylate (TMPTA) as a crosslinker, and 4.70 wt% Hypermer B246-SO-M as a surfactant. The mixture was heated to 50 °C until the surfactant was completely dissolved. Beta-carotene (0.02 wt%) and tartrazine (0.06 wt%), based on the total mass of the continuous phase, were then incorporated as optical absorbers to control light penetration during photopolymerization. Subsequently, 5 wt% photoinitiator was added to the continuous phase. The emulsion was formed by gradually introducing distilled water (dH_2O) as the internal phase at 80 vol.% and 87.5 vol.%, while maintaining constant stirring at 300 rpm using a SciQuip-Pro 40 stirrer, resulting in emulsions with two distinct porosities.

2.2. Additive Manufacturing of Porous Polymers

PolyHIPE lattices were fabricated using a digital light processing (DLP) 3D printer (Elegoo Mars 3 Pro). The cubic vertex centroid

lattice geometry (hereafter referred to as the lattice structure) was sourced from Thingiverse.com and modified in Autodesk Fusion 360 to include a supporting base. The final models were exported in STL format and prepared for printing using CHITUBOX Basic slicing software. Lattice specimens measuring 18 mm × 18 mm × 20 mm, including a 20 mm × 20 mm × 3 mm base, were printed with a layer thickness of 60 µm and an exposure time of 8 s. Following fabrication, the printed structures were cleaned in methanol to remove uncured resin and other residual polyHIPE components, then oven-dried at 65 °C for 24 hours to ensure complete solvent evaporation.

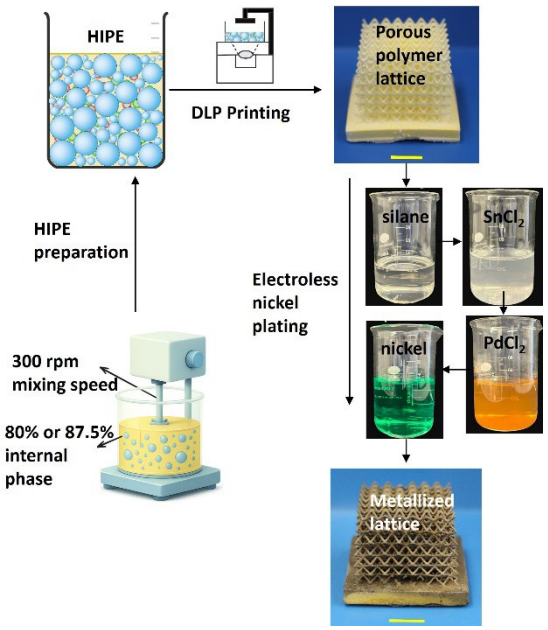

Figure 1. Schematic overview of the composite lattice fabrication process, illustrating the 3D printing of the CVC polyHIPE template via vat photopolymerization, subsequent surface sensitization and activation steps, and the final electroless nickel plating process.

2.3. Electroless Nickel Coating of 3D-Printed PolyHIPE Lattices

Prior to metallization, the surfaces of the polyHIPE structures were functionalized to improve hydrophilicity and subsequently activated to facilitate nickel deposition. Initially, the samples were immersed in 3-(trimethoxysilyl)propyl methacrylate (TMPSM) at 40 °C for 15 minutes, followed by oven drying at 65 °C until fully dehydrated (approximately 48 hours). The silane-treated polyHIPEs were then sequentially immersed in $SnCl_2$ and $PdCl_2$ solutions at 40 °C for 20 minutes and 10 minutes, respectively. The $SnCl_2$ solution was prepared by combining 0.8 wt% $SnCl_2$, 100 mL deionized water (dH_2O), and five drops of HCl, while the $PdCl_2$ solution consisted of 0.06 wt% $PdCl_2$, 2 wt% H_3BO_3, 100 mL dH_2O, and eight drops of HCl. The pH values of the $SnCl_2$ and $PdCl_2$ solutions were adjusted to 1.2 and 1.7, respectively. Each treatment used 100 mL of solution to process six discs and three lattice samples, ensuring minimal cross-contamination.

The electroless nickel plating bath was subsequently prepared by diluting Caswell plating solutions (Part A and Part B) with deionized water in the proportions of 5 vol.% Part A, 15 vol.% Part B, and 80 vol.% dH_2O. The activated polyHIPE specimens were immersed in the plating bath at 90 °C for 30 minutes to achieve uniform nickel deposition. A schematic illustration summarizing the overall experimental workflow, from the vat photopolymerization of the lattices to the surface activation and final electroless nickel deposition, is presented in Figure 1.

2.4. Characterization

The bulk density of the lattices was measured using mercury intrusion porosimetry (MIP). Due to the high accuracy, precision, and low margin of error characteristic of this analytical technique, single representative measurements were recorded for the samples.

The internal architecture and surface features of both non-metallized and nickel-coated polyHIPE samples were characterized using scanning electron microscopy (SEM). To prevent surface charging during imaging, the non-metallized specimens were sputter-coated with a thin layer of gold, and observations were carried out at an accelerating voltage of 5 kV.

Pore size quantification was conducted using ImageJ software, and a statistical correction factor ($2/\sqrt{3}$) was applied to the measured diameters to account for the underestimation associated with random cross-sectional cuts. The penetration depth of the Ni coating was defined as the continuous perpendicular distance from the outer exterior surface of the lattice toward the core where the metallic layer was visibly continuous on the internal pore walls. Measurements were conducted using ImageJ software on cross-sectional SEM micrographs. For each experimental group (n=3

replicates), data were collected from 5 distinct locations per specimen, and the values were reported as the mean ± standard deviation.

Elemental composition of the metallized samples was analyzed using SEM coupled with an energy-dispersive X-ray spectroscopy (EDS) detector, operated at an accelerating voltage of 20 kV.

To assess the mechanical performance of the lattices, uniaxial compression tests were performed on both non-metallized and metallized samples at a crosshead speed of 1 mm/min. For mechanical analysis, the compressive modulus was calculated from the slope of the initial macroscopic linear elastic region of the stress-strain curves, specifically targeting the 0% to 5% compressive strain interval. Given the distinct mechanical behaviors of the samples, the compressive strength was defined as the first maximum peak stress prior to structural yielding for the rigid metallized lattices (P80Ni). For the non-metallized templates (P80) that did not exhibit a distinct yield peak, the compressive strength was evaluated at 10% compressive strain in accordance with standard testing protocols for cellular plastics (ISO 844 / ASTM D1621).

All data processing and statistical analyses were performed using OriginPro 2024, which was also used to calculate the mean and standard deviation values. The number of replicates (n) for each experiment is reported in the corresponding figure legends.

3. RESULTS AND DISCUSSION

3.1. Pore Morphology of As-Printed Lattices

SEM images (Figure 2) show the characteristic open-cell morphology that is typical of polyHIPE structures. Both the 80% (P80) and 87.5% (P87.5) porosity polyHIPE lattices exhibited interconnected pores with near-spherical geometry and thin polymer struts (Figure 3), confirming successful emulsion templating during vat photopolymerization.

The pore size data obtained from image analysis indicate that the average pore diameters were 35.15 ± 17.47 µm for P80 and 41.55 ± 14.20 µm for P87.5, respectively. The increase in average pore size with higher internal phase content aligns with previous reports on emulsion-derived polymers, where higher dispersed-phase volumes lead to coalescence of droplets and the formation of larger voids [4–6].

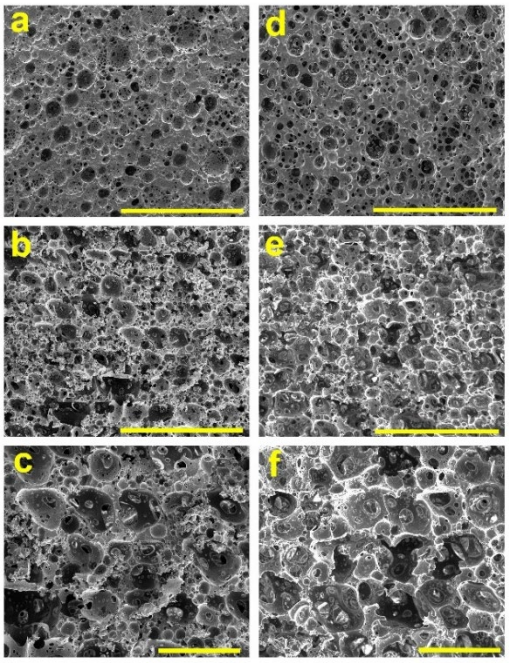

Figure 2. Pore morphology of as-printed 3D polyHIPE lattices. Surface SEM images of the **(a)** 80% and **(d)** 87.5% porosity samples. Cross-section SEM images of the **(b, c)** 80% and **(e, f)** 87.5% porosity samples and lower and higher magnifications. Scale bars are 300 µm in **(a), (b)**, **(d)** and **(e)** and 100 µm in **(c)** and **(f)**. (n=3).

The open surfaces and interconnected porosity provided continuous pathways through the lattice struts, which is beneficial for subsequent metallization processes, as it facilitates the penetration of the electroless plating solution into the porous network. No significant collapse or deformation of the lattice architecture was observed after the washing and drying stages, indicating that the printed polyHIPEs retained sufficient structural integrity for further surface treatments.

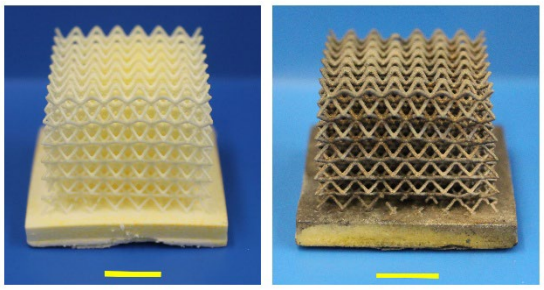

Figure 3. Additively manufactured 3D polyHIPE (left panel) and metallized (right panel) lattices. Scale bars are 10 mm.

3.2. Surface and Cross-Sectional Characterization of Metallized Lattices

Nickel coated 80% (P80Ni) and 87.5% (P87.5Ni) porosity lattices retained their architecture after metallization (Figure 3). SEM–EDS analyses (Figures 4 - 7) confirmed the successful deposition of nickel coatings on both polyHIPE lattices.

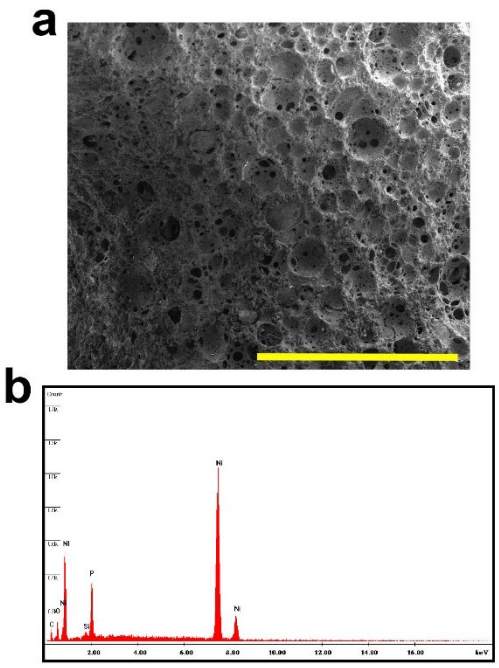

Figure 4. (a) SEM images of surface morphology after Ni plating for 80% porosity sample. **(b)** EDS spectra confirming the presence of nickel on the surface of the samples. Scale bar is 300 µm.

The metallic sheen of the Ni-coated samples indicated the uniformity of the electroless plating process. SEM surface images demonstrated that the Ni layer formed a conformal and continuous coating across the porous skeleton without compromising the open-cell morphology.

EDS spectra (Figure 4b and Figure 5b) verified the presence of nickel as the dominant surface element, accompanied by minor signals from phosphorus, oxygen, and carbon. The phosphorus peak originated from the hypophosphite reducing agent, which typically leads to amorphous Ni–P coatings known for enhanced corrosion resistance [20].

Cross-sectional SEM images (Figures 6a–b and Figures 7a–b) revealed that the nickel coating effectively penetrated the internal pore walls of the lattice. The nickel penetration depths for P80 and P87.5 were 83 ± 21 µm and 199 ± 86 µm, respectively. The greater porosity of the P87.5 lattice facilitated deeper coating penetration due to its larger pore size. The coating thickness appeared uniform across the section, consistent with the self-limiting nature of electroless deposition.

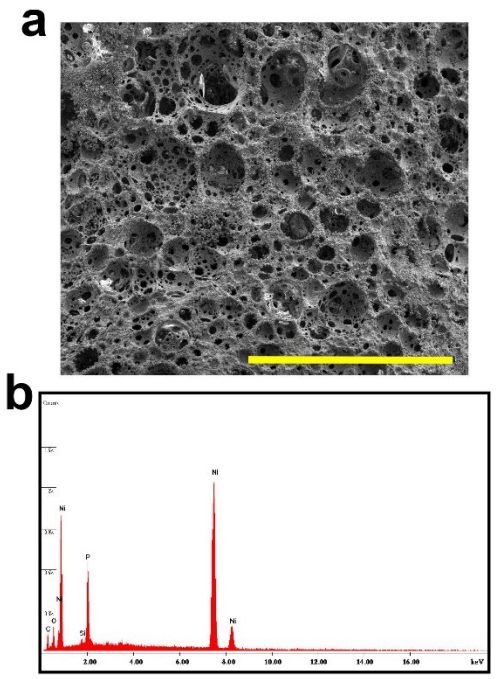

Figure 5. (a) SEM image of surface morphology after Ni plating for 87.5% porosity samples. **(b)** EDS spectra confirming the presence of nickel on the surface of the sample. Scale bar is 300 µm.

EDS spectra obtained from the cross-sectional regions (Figure 6c and Figure 7c) further confirmed the presence of nickel throughout the coating layer for both porosity levels. The Ni peak intensity was higher for P87.5Ni compared to P80Ni, indicating a greater degree of metallization across the cross-section. Conversely, the C peak intensity was higher for P80Ni, suggesting a greater proportion of polymer substrate relative to the Ni coating.

Overall, the metallization process yielded uniform, well-adhered nickel coatings across the external and internal surfaces of the polyHIPE lattices, demonstrating the effectiveness of electroless plating in reinforcing inherently porous polymer structures. Moreover, the higher-porosity (87.5%) lattices exhibited deeper coating penetration, indicating that increased porosity facilitates more effective metallization.

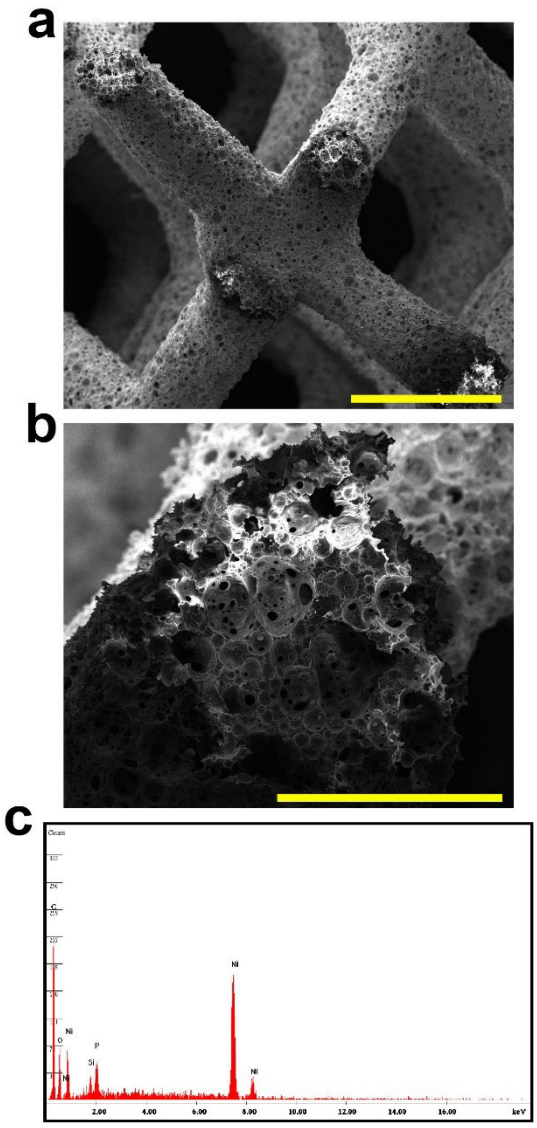

Figure 6. Cross-sectional analysis of metallized lattices. **(a, b)** SEM cross-section of the 80% porous sample showing nickel coating penetration at lower and higher magnifications. **(c)** EDS spectrum from the cross-section of the 80% sample. Scale bars are 1 mm in **(a)** and 300 µm in **(b)**. (n=3).

3.3. Comparison of the Mechanical Properties of Metallized and Non-Metallized Lattices

While both porosity levels were evaluated for structural and coating penetration characteristics, the P80 lattice was selected as the representative reference model to quantitatively evaluate the mechanical strengthening effect of the metallization process. The compressive stress–strain responses of non-metallized (P80) and metallized (P80Ni) lattices are presented in Figure 8.

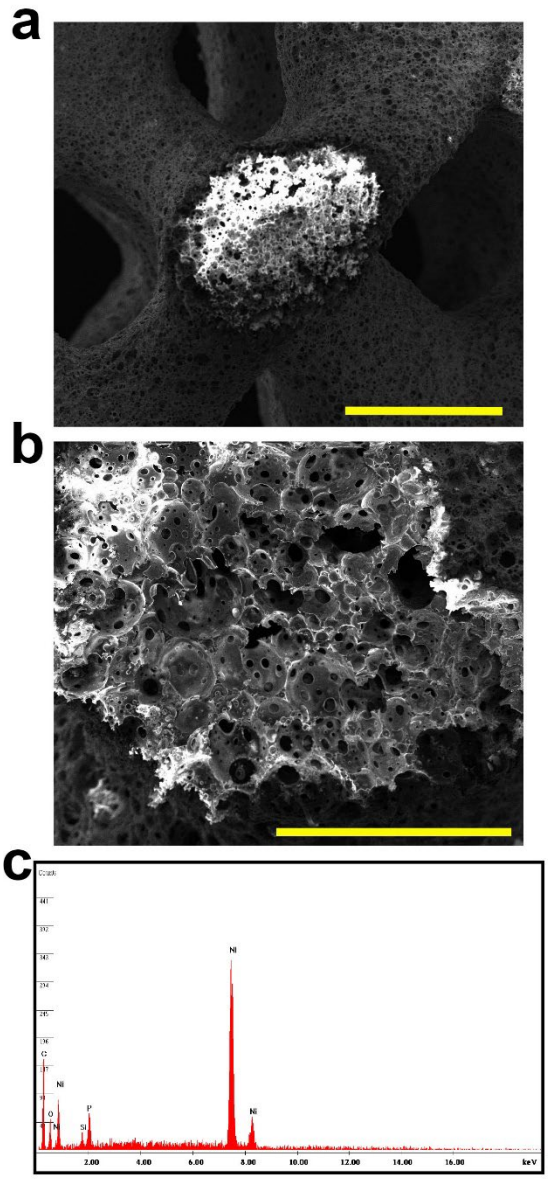

Figure 7. (a, b) SEM cross-section of the 87.5% porous sample showing nickel coating penetration at lower and higher magnifications. **(c)** EDS spectrum from the cross-section of the 87.5% sample. Scale bars are 1 mm in **(a)** and 300 µm in **(b)**. (n=3).

The uncoated polyHIPE lattices exhibited typical elastomeric deformation behavior with low compressive modulus and gradual densification at higher strains. In contrast, the nickel-coated lattices showed a pronounced increase in load-bearing capacity, with compressive modulus increasing from 0.27 ± 0.06 kPa to 159.70 ± 29.26 kPa upon metallization. This represents a substantial enhancement in the compressive modulus. It is noteworthy that the uncoated P80 lattice exhibited an extremely low compressive

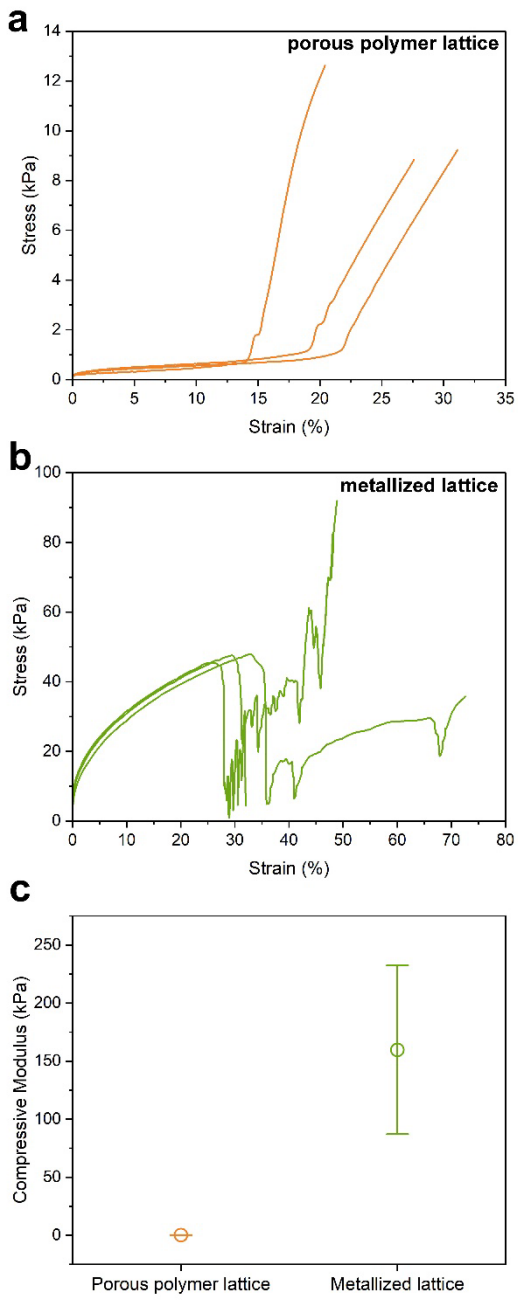

Figure 8. Mechanical performance of 80% porous 3D printed lattices. Stress–strain curves of **(a)** non-metallized and **(b)** Ni-metallized samples. **(c)** Comparison of the compressive modulus values of non-metallized and Ni-metallized samples, demonstrating the effect of metallization. (n=3).

modulus, behaving essentially as an elastomeric sponge. The application of the electroless nickel coating transformed this highly flexible framework into a structurally rigid composite, achieving an extraordinary ~590-fold increase in modulus. Beyond the evaluation of the compressive modulus, the compressive strength was analyzed to provide a more comprehensive mechanical profile of the lattices. The uncoated P80 framework exhibited a baseline compressive strength of only 0.55 ± 0.08 kPa, further reflecting its flexible and sponge-like nature. Following the electroless nickel deposition, the P80Ni composite demonstrated a drastic increase in its load-bearing capacity, reaching a compressive strength of 47.14 ± 0.92 kPa. The 85-fold boost in strength, combined with the higher modulus, clearly shows how the flexible polymer became a robust metal-reinforced architecture. These results confirm that the conformal metallic layer not only stiffens the framework but also significantly improves its resistance to structural yielding.

The dramatic strengthening effect is attributed to the presence of the continuous metallic coating that efficiently transfers and distributes the applied load through the porous framework [15, 21–23]. The metallic layer also constrains localized deformation of the polymer struts, thereby preventing early collapse and improving the overall energy absorption capacity. Such trends are consistent with previous studies reporting mechanical reinforcement of polymeric lattices through metallic coating or infiltration [21–26].

The mechanical data confirm that electroless nickel plating effectively converts lightweight polyHIPE lattices (0.40 g cm^{-3}) into stiff, load-bearing architected materials (0.71 g cm^{-3}), while preserving their low density and open porosity. Furthermore, the specific compressive modulus increased drastically from ~0.68 kPa/(g cm^{-3}) for P80 to ~223.94 kPa/(g cm^{-3}) for P80Ni, confirming that the conformal metallic coating acts as a robust exoskeleton.

3.4. Structure–Property Relationships

The structural analysis indicates that porosity plays a critical role in determining coating behavior, while the mechanical analysis of the representative P80 series demonstrates that metallization significantly enhances the overall mechanical performance. The bulk density increased from 0.40 g cm^{-3} to 0.71 g cm^{-3} upon metallization, reflecting the successful deposition of the conformal nickel layer. Although both porosity levels (80% and 87.5%) were successfully nickel coated, the larger-pore P87.5 lattices exhibited deeper nickel penetration, indicating that increased pore size promotes coating uniformity.

The mechanical reinforcement was particularly remarkable for the P80 series, the compressive modulus increased from 0.27 ± 0.06 kPa to 159.70 ± 29.26 kPa (an extraordinary ~590-fold increase), while the compressive strength increased from 0.55 ± 0.08 kPa to 47.14 ± 0.92 kPa (an ~85-fold increase). These findings confirm that controlled emulsion templating during vat photopolymerization, followed by electroless nickel plating, enables precise tuning of mechanical properties while preserving the material's inherently low density and open porosity.

The transformation of the flexible polymer template into a structurally robust composite confirms that the conformal metallic coating acts as a load-bearing exoskeleton. This processing route provides a versatile strategy for fabricating multifunctional architected materials that combine low weight, high compressive modulus, and tunable surface functionality, making them promising candidates for lightweight structural, catalytic, and energy-related applications.

4. CONCLUSION

In this study, inherently porous polymer lattices were fabricated using a high internal phase emulsion (HIPE) formulation through vat photopolymerization and subsequently reinforced via electroless nickel plating. Two porosity levels (80% and 87.5%) were investigated to assess the influence of porosity on metallization behavior and mechanical performance. Scanning electron microscopy (SEM) imaging demonstrated open-cell, interconnected pore structures characteristic of polyHIPEs, with mean pore size of 35.15 ± 17.47 μm and 41.55 ± 14.20 μm, respectively. Electroless nickel plating produced uniform and conformal coatings across both surface and internal pore walls, as confirmed by energy-dispersive X-ray spectroscopy (EDS). Cross-sectional analyses indicated improved coating penetration in higher-porosity lattices. The novelty of this work lies in the successful reinforcement of an intact polymer template rather than its removal and in providing the first detailed mechanical characterization of metallized complex lattice geometries as opposed to simple solid specimens. Mechanical testing demonstrated a substantial improvement in compressive modulus from 0.27 ± 0.06 kPa to 159.70 ± 29.26 kPa, and an 85-fold increase in compressive strength from 0.55 ± 0.08 kPa to 47.14 ± 0.92 kPa upon metallization. The results highlight a strong correlation between porosity and penetration depth, while the quantitative mechanical data confirm the effectiveness of electroless plating in converting lightweight porous polymers into structurally robust, multifunctional architected materials suitable for advanced engineering applications.

ACKNOWLEDGES

This work was partially supported by the Scientific and Technological Research Council of Turkey (TÜBİTAK) through the 1002-A Short term Support Module (125M827).

REFERENCES

1. Silverstein, M. S., "PolyHIPEs: Recent advances in emulsion-templated porous polymers", Progress in Polymer Science, Vol. 39, Issue 1, Pages 199–234, 2014.

2. Wu, J., Xu, F., Li, S., Ma, P., Zhang, X., Liu, Q., Fu, R., Wu, D., "Porous polymers as multifunctional material platforms toward task-specific applications", Advanced Materials, Vol. 31, Issue 4, Pages 1802922, 2019.

3. Guo, Z., Zhou, C., "Recent advances in ink-based additive manufacturing for porous structures", Additive Manufacturing, Vol. 48, Pages. 102405, 2021.

4. Silverstein, M. S., "Emulsion-templated polymers: Contemporary contemplations", Polymer, Vol. 126, Pages 261–282, 2017.

5. Aldemir Dikici, B., Claeyssens, F., "Basic Principles of Emulsion Templating and Its Use as an Emerging Manufacturing Method of Tissue Engineering Scaffolds", Frontiers in Bioengineering and Biotechnology, Vol. 8, Pages. 554312, 2020.

6. Durgut, E., Claeyssens, F., "Pickering polymerized high internal phase emulsions: Fundamentals to advanced applications", Advances in Colloid and Interface Science, Vol. 336, Pages. 103375, 2025.

7. Liu Q, Xiong J, Lin W, Liu J, Wan Y, Guo CF, Wang Q, Liu Z., "Porous polymers: structure, fabrication and application", Materials Horizons, Vol. 12, Issue 8, Pages 2436–2466, 2025.

8. Wu Y., Huang J., Guo Z., Yang Q., Xia C., Zheng Z., "Preparation of Polymerized High Internal Phase Emulsion Membranes with High Open-Cellular Extent and High Toughness via RAFT

Polymerization", Polymers, Vol. 17, Issue 4, Pages 515, 2025.

9. ISO/ASTM 52900:2021(en), "Additive manufacturing — General principles — Fundamentals and vocabulary", https://www.iso.org/obp/ui/#iso:std:iso-astm:52900:ed-2:v1:en, October 28, 2025.

10. Goh, G.D., Yap, Y.L., Tan, H.K.J., Sing, S.L., Goh, G.L., Yeong, W.Y., "Process–Structure–Properties in Polymer Additive Manufacturing via Material Extrusion: A Review", Critical Reviews in Solid State and Materials Sciences, Vol. 45, Issue 2, Pages. 113–133, 2020.

11. Sears, N. A., Dhavalikar, P. S., Cosgriff-Hernandez, E. M., "Emulsion Inks for 3D Printing of High Porosity Materials", Macromolecular rapid communications, Vol. 37, Issue 16, Pages 1369–1374, 2016.

12. Sears, N., Dhavalikar, P., Whitely, M., Cosgriff-Hernandez, E., "Fabrication of biomimetic bone grafts with multi-material 3D printing", Biofabrication, Vol. 9, Issue 2, Pages 025020, 2017.

13. Yang, T., Hu, Y., Wang, C., Binks, B. P., "Fabrication of Hierarchical Macroporous Biocompatible Scaffolds by Combining Pickering High Internal Phase Emulsion Templates with Three-Dimensional Printing", ACS Applied Materials & Interfaces, Vol. 9, Issue 27, Pages 22950–22958, 2017.

14. Sherborne, C., Owen, R., Reilly, G. C., Claeyssens, F., "Light-based additive manufacturing of PolyHIPEs: Controlling the surface porosity for 3D cell culture applications", Materials & Design, Vol. 156, Pages 494–503, 2018.

15. Sengokmen-Ozsoz, N., Boston, R., Claeyssens, F., "Investigating the Potential of Electroless Nickel Plating for Fabricating Ultra-Porous Metal-Based Lattice Structures Using PolyHIPE Templates", ACS Applied Materials & Interfaces, Vol. 15, Issue 25, Pages 30769–30779, 2023.

16. Ghosh, S., Yadav, A., Rani, S., Takkar, S., Kulshreshtha, R., Nandan, B. and Srivastava, R.K., "3D Printed Hierarchical Porous Poly(ε-caprolactone) Scaffolds from Pickering High Internal Phase Emulsion Templating", Langmuir, Vol. 39, Issue 5, Pages 1927–1946, 2023.

17. Sengokmen-Ozsoz, N., Boston, R., Dean, J.S., Rodenburg, C., Claeyssens, F., "Fabrication of hierarchically porous carbon lattices derived from 3D-Printed polymerized high internal phase mulsions", Carbon, Vol. 234, Pages 119933, 2025.

18. Sengokmen-Ozsoz, N., Aleemardani, M., Palanca, M., Hann, A., Reilly, G.C., Dall'Ara, E., Claeyssens, F., "Fabrication of hierarchically porous trabecular bone replicas via 3D printing with high internal phase emulsions (HIPEs)", Biofabrication, Vol. 17, Issue 1, Pages 015012, 2024.

19. Li, L., Liu, B., "Study of Ni-catalyst for electroless Ni–P deposition on glass fiber", Materials Chemistry and Physics, Vol. 128, Issue 1–2, Pages 303–310, 2011.

20. Loto, C. A., "Electroless Nickel Plating – A Review", Silicon, Vol. 8, Issue 2, Pages 177–186, 2016.

21. Schaedler, T.A., Jacobsen, A.J., Torrents, A., Sorensen, A.E., Lian, J., Greer, J.R., Valdevit, L., Carter, W.B., "Ultralight metallic microlattices", Science, Vol. 334, Issue 6058, Pages 962–965, 2011.

22. Maloney, K.J., Roper, C.S., Jacobsen, A.J., Carter, W.B., Valdevit, L., Schaedler, T.A., "Microlattices as architected thin films: Analysis of mechanical properties and high strain elastic recovery", APL Materials, Vol. 1, Issue 2, Pages 022106, 2013.

23. Xu, J., Gao, Y., Huang, H., Yang, Q., Guo, L., Jiang, L., "Diamond-structured hollow-tube lattice Ni materials via 3D printing", Science China Chemistry, Vol. 59, Issue 12, Pages 1632–1637, 2016.

24. Fan, Q., Gao, Y., Zhao, Y., Yang, Q., Guo, L., Jiang, L., "Fabrication of diamond-structured composite materials with Ni-P-diamond particles by electroless plating", Materials Letters, Vol. 215, Pages 242–245, 2018.

25. Xiao, L., Feng, G., Li, S., Mu, K., Qin, Q., Song, W., "Mechanical characterization of additively-manufactured metallic lattice structures with hollow struts under static and dynamic loadings", International Journal of Impact Engineering, Vol. 169, Pages 104333, 2022.

26. Liu, J., Zhao, X., Yang, Q., Wang, K., Fu, Y., Yang, Q., "Particle-reinforced ultralight hollow Ni-P-B4C microlattice composite materials", Materials Letters, Vol. 331, Pages 133438, 2023.

27. Dai, G., Wu, S., Huang, X., Zhang, X., Wang, M., "A novel strategy for designable alloy coatings in electroless plating", Transactions of the IMF, Vol. 101, Issue 2, Pages 101–112, 2023.